ORIGINAL ARTICLE

Effects of Variation of Axial Load on Seismic Performance of Shear Deficient RC Exterior BCJs

Mohammed Ali Al-Osta[1*] , Umais Khan[1], Mohammed Hussain Baluch[1] and Muhammad Kalimur Rahman[2]

Abstract

The focus of this paper is to investigate the effect of column axial load levels on the performance of shear deficient reinforced concrete beam column joints (BCJs) under monotonic and cyclic loading. The problem of interaction between shear stress in BCJ and axial load on column has been addressed in this work by initially postulating a mechanistic model and substantiated by an experimental test program. This was achieved by conducting appropriate tests on seven BCJ sub-assemblies subjected to monotonic and reversed cyclic loading, with varying levels of the column axial load. Experimental results were further validated using a finite element model in an ABAQUS environment. The effect of variation of compressive strength of concrete was considered in a subsequent parametric study, in order to obtain sufficient data, and utilized to develop a new shear strength model for BCJs which includes influences of all the important parameters required to predict the shear strength of BCJs. The results showed that column axial load affects the seismic performance of BCJs significantly. Experimental results demonstrated that at initial stages of loading, increase in axial load enhances the shear capacity of the joint and reduces its ductility. However, when the column axial load/axial strength ratio increases to about 0.6–0.7, shear strength starts to decrease rapidly, leading to pure axial failure of the joint. The magnitude of axial load/axial capacity ratio also dictates the failure mode and development of crack patterns in BCJs. Results of reverse cyclic tests on BCJs showed that high value of axial load/axial capacity ratio increases the initial stiffness of BCJ but rate of stiffness degradation is accelerated after peak strength attenuation.

Keywords: shear failure, beam-column joints, axial load, monotonic, reverse cyclic tests, finite element model, mechanistic model

1 Introduction

Since the 1970s there have been many developments in the field of earthquake engineering, resulting in advanced seismic design codes and regulations that were developed for different structural components, including beam column joints (BCJs). Many researchers have studied parameters that influence the performance of BCJs such as the aspect ratio, material properties, beam reinforcement ratio, anchorage of beam reinforcement, and the confinement effect of the presence of slab and transverse beams. The influence of these parameters is well understood, and has been incorporated in several joint shear strength models and consequently guidelines for design are available in the current design guidelines. However, effect of magnitude of column axial load, which is a key influencing parameter in predicting shear strength of BCJs, has not been considered explicitly thus far, and its complex effects on the shear strength of the joint remained not well understood.

Sparse information is present in literature regarding the effect of column axial load in predicting seismic performance of BCJ. Research work by Pantelides et al. (2002), Barnes and Jigoral (2008), Wong (2005), Antonopoulos and Triantafillou (2003), Pantelides et al. (2008) and Sarsam and Phillips (1985) concluded that an increase in the column axial load also improves the shear capacity of BCJ. However, the range of column axial load/axial

*Correspondence: malosta@kfupm.edu.sa
[1] Civil and Environmental Engineering Department, King Fahd University of Petroleum and Minerals (KFUPM), Dhahran 31261, Saudi Arabia
Full list of author information is available at the end of the article

Al-Osta *et al. Int J Concr Struct Mater* (2018) 12:46

Page 2 of 20

strength ratio considered by above researchers is very narrow and it is usually less than 0.15. The maximum axial load considered and well documented in the form of shear strength equation is 0.42 f_c' A$_g$ as in the case of Sarsam and Phillips (1985). Masi et al. (2014) conducted experimental work on full-scale beam-column joints with wide beam to study the effect of axial load on the behavior of BCJ; the values of axial load ratio considered were 0.15 and 0.3. The results showed that the deformation and ductility are affected by the magnitude of column axial load. Li et al. (2015) studied the effect of high axial load on the non-seismically designed RC BCJ with or without strengthening. The ratios of axial load considered were 0.2 and 0.6. Masi et al. (2013) also conducted experimental work on beam-column joints to study influence of a known axial load on the column, dimensions of the beam, and steel on behavior of BCJ. Tran (2016) analyzed data published from literature of a total of 172 experimental works on BCJ. The results showed that the effect of column axial load on the joint shear strength of BCJ was higher for the exterior joint than that of the interior joint. Another group of researchers like Vollum and Newman (1999), Bakir and Boduroglu (2002) believe that the axial load on the column does not affect joint shear strength.

The main emphasis of this research work was to investigate the effect of column axial load levels on the performance of reinforced concrete BCJs under monotonic and cyclic loading and to develop shear strength model that considers all important parameters including column axial load, beam reinforcement ratio, concrete compressive strength and aspect ratio of BCJ. Surprisingly, no shear strength model is available in literature that combines all the above influencing parameters together that would yield a more representative and conservative estimate of BCJs shear strength.

2 Evaluation of Existing BCJ's Shear Strength Models

Several BCJ shear strength models are available in literature to characterize its behavior under seismic loading. In this section, the existing joint shear strength models proposed by several researchers and design guidelines are reviewed.

Vollum and Newman (1999) have developed a shear strength model to predict the shear capacity of exterior BCJs. Their model while considering the influence of anchorage details of beam longitudinal reinforcement into the joint and joint aspect ratio as significant parameters did not explicitly consider the effect of column axial load.

Bakir and Boduroglu (2002) proposed an empirical model considering mainly the effect of anchorage details,

amount of beam longitudinal reinforcement and aspect ratio of joint. The effects of above parameters are incorporated in their model based on parametric study and by calibrating each parameter independently from the other. The proposed shear strength equation is as follows:

$$V_c = 0.17\beta\gamma \left(\frac{100A_{sb}}{b_b d}\right)^{0.4289} \left(\frac{b_c + b_b}{2}\right) \left(\frac{h_b}{h_c}\right)^{-0.61} \times h_c \sqrt{f_c} \ (Newtons) \tag{1}$$

where β can be taken as 0.85 for joints with U shaped anchorage of beam reinforcement and 1 for the standard 90-degree hook. γ can be taken as 1.37 for inclined bars in the joint and 1 for other cases, b_b is the width of beam, b_c is the width of column, h_b is the depth of beam, h_c is the depth of column, A_{sb} is area of beam longitudinal reinforcement whereas f_c is the compressive strength of concrete. The proposed joint shear strength equation does not take into account the effect of axial load on the column. According to the analysis of Bakir and Boduroglu (2002), column axial load magnitude has no effect on the joint shear strength.

Sarsam and Phillips (1985) proposed a shear strength model based on test databank of exterior BCJs subjected to monotonic loading. Parameters like the aspect ratio of joint, axial load on column and column steel percentage are considered. According to this model, joint shear capacity increases with an increase in an axial load. However, a limit of axial load ratio $\frac{N}{A_g f_c'} \leq 0.42$ was set due to non-availability of experimental results in literature above this limit.

ACI-ASCE Committee 352 (2002) recommended the following joint nominal shear strength equation:

$$V_n = 0.083\gamma \sqrt{f_c'} \ b_j h_c \ (Newtons) \tag{2}$$

where V_n is the shear strength of joint, γ is a value that depends on the connections classification and seismic magnitude, b_j is the effective joint width, and h_c is the depth of the column in the direction of joint shear being considered. These guidelines do not account for the influence of column axial load in predicting shear strength of joints.

3 Mechanics of BCJ's

A mechanistic model to predict the shear strength of beam column joints under various levels of column axial load was initially developed by the authors in an earlier project (Al-Osta et al. 2017). The column axial load N creates an axial stress σ_N whereas load on beam V creates shear stresses τ_v in the joint. These stresses can be

Al-Osta *et al. Int J Concr Struct Mater* (2018) 12:46

Page 3 of 20

converted to principal joint stresses σ_1 and σ_2 using Mohr's circle as:

Principal joint stresses can be calculated as follows:

$$\sigma_1 = \frac{\sigma_x + \sigma_y}{2} + \sqrt{\left(\frac{\sigma_x - \sigma_y}{2}\right) + \tau_{xy}^2} \tag{3}$$

$$\sigma_2 = \frac{\sigma_x + \sigma_y}{2} - \sqrt{\left(\frac{\sigma_x - \sigma_y}{2}\right)^2 + \tau_{xy}^2} \tag{4}$$

with $\sigma_x = \sigma_N$ and $\sigma_y = 0$, Eqs. (3) and (4) can be written as:

$$\sigma_1 = \frac{\sigma_N}{2} + \sqrt{\left(\frac{\sigma_N}{2}\right)^2 + \tau_{xy}^2} \tag{5}$$

$$\sigma_2 = \frac{\sigma_N}{2} - \sqrt{\left(\frac{\sigma_N}{2}\right)^2 + \tau_{xy}^2} \tag{6}$$

As per Mohr–Coulomb failure criteria, two strength parameters, tensile strength, f_t and compressive strength, f_c' are required to define the failure surface of concrete. The Mohr–Coulomb failure surface is shown in Fig. 1 for a plane stress environment in which the equation of the failure locus in the fourth quadrant can be expressed as:

$$\frac{\sigma_1}{f_t} - \frac{\sigma_2}{f_c'} = 1 \tag{7}$$

Along any stress path

$$\sigma_2 = c\sigma_1 \tag{8}$$

Where the range of $1/c$ is $[-1, 0]$.
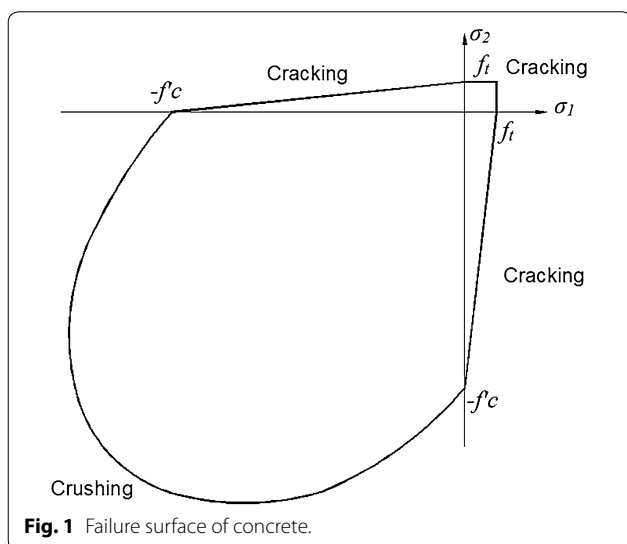
Substituting Eq. (8) into Eq. (7), σ_1 and σ_2 can be written as:

$$\sigma_1 = \frac{f_c f_c'}{f_c' - c f_t} \tag{9}$$

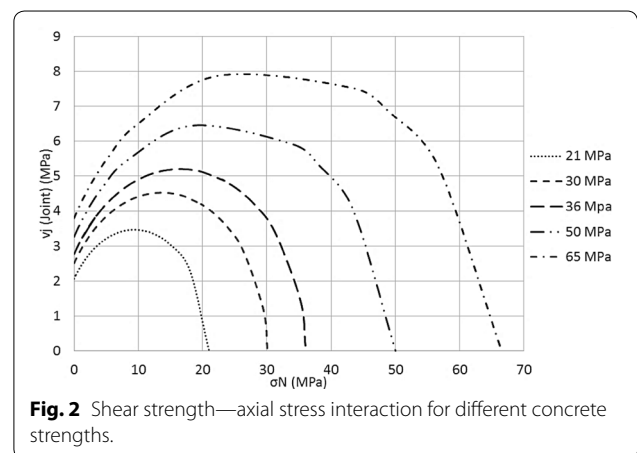$$\sigma_2 = \frac{c f_t f_c'}{f_c' - f_t} \tag{10}$$

Solving Eqs. (5) and (9) or Eqs. (6) and (10) simultaneously with various values of σ_N in the range $[0, -f_c']$ and $1/c$ range $[-1, 0]$, shear stress at failure can be obtained for each value of σ_N. Thus, plotting σ_N against the calculated value of $\tau_{xy} = v_j$, the interaction diagram as shown in Fig. 2 can be established for various strengths of concrete.

4 Experimental Program

The experimental program was designed to include load tests on seven 1/3 scale exterior BCJs. Both monotonic and reversed cyclic loading was considered in the test program to estimate the actual shear capacity and to evaluate stiffness degradation pattern under seismic excitation. Monotonic tests were performed on four specimens to monitor the influence of different magnitude of column axial loads on the joint shear strength and failure mechanism, whereas reversed cyclic loading was applied on three BCJs to understand the ductility, strength degradation and energy dissipation capacity of BCJ.

4.1 Specimen Design

The BCJ dimensions and reinforcement details were kept constant in all seven specimens designed on a scale of 1/3. There was no transverse reinforcement present in any of the BCJ. The reinforcement ratio in a beam was kept high to promote joint shear failure mechanism and to avoid beam reinforcement yielding. Development length and anchorage details of

Fig. 1 Failure surface of concrete.

Fig. 2 Shear strength—axial stress interaction for different concrete strengths.

Al-Osta *et al. Int J Concr Struct Mater* (2018) 12:46

Page 4 of 20

beam longitudinal reinforcement satisfied ACI Committee, 318-14 (2014) to ensure proper shear transfer from beam to the joint. The column was designed such that its flexural capacity was considerably greater than demand imposed by the load on the beam for a joint shear failure. Details of beam and column design are tabulated in Table 1 whereas Fig. 3 shows the beam column joint dimensions and reinforcement layout in the specimens.

4.2 Material Properties
Compressive strength test of concrete was conducted on test date of each specimen according to ASTM C39 M at a loading rate of 0.25 MPa/s. Three cylinders were tested for each specimen and the average compressive strengths

was calculated as 21 MPa except for specimens SP-6 and SP-7 where it was 30 MPa.

ASTM A615 deformed reinforcement was utilized for column and beam reinforcements. Tensile strength test results of steel reinforcement are summarized in Table 2.

4.3 Test Setup Details
Test setup is designed to simulate forces and boundary conditions to which BCJ is subjected under seismic excitation. Moment release is provided at beam's end and at top and bottom ends of the column to simulate the three inflection points in the actual structure as shown in Fig. 4a which is the deformed shape of BCJ sub-assembly under seismic action where L is the length of the beam, L_c is the length of the column, L_b is the length of beam

Table 1 Beam and column design details.

Specimen	Dimensions (mm)		Reinforcement				
			Beam			Column	
			Top	Bottom	Stirrups	Main	Ties
SP1-SP7	Beam	Column	4 Ø20	4 Ø20	Ø8 @ 50	6 Ø20	Ø8 @ 50
	200 × 250	200 × 250					
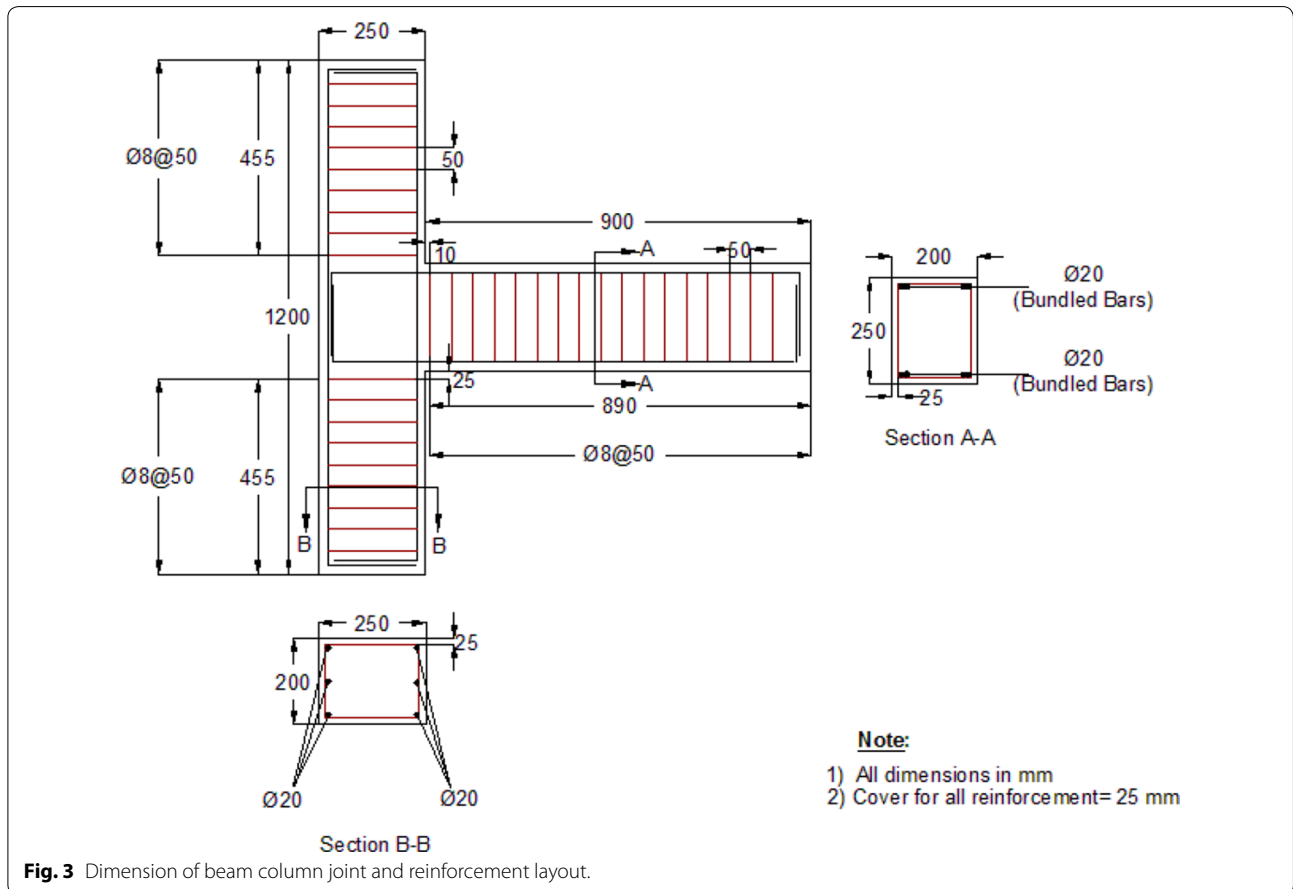
Fig. 3 Dimension of beam column joint and reinforcement layout.

Al-Osta *et al. Int J Concr Struct Mater* (2018) 12:46

Page 5 of 20

Table 2 Results of steel tensile test.

Specimen	Bar size (mm)	Stress (MPa)		Strain με (Micro strain)	
		f_y	f_u	ϵ_y	ϵ_u
SP1-SP7	Ø8	580	667	3000	10,500
	Ø20	605	695	3100	10,600

considered in the test, N is the axial load on column, V_{col} is the column shear, Δ_H is the horizontal drift, Δ and P are the imposed displacement and load at the tip of the beam respectively. Figure 4b shows the idealized testing arrangement in which both ends of the column are restrained with pin while the push and pull load at beam tip is applied to simulate load reversal that occurs due to alternating lateral drift and which perfectly simulates the forces and boundary conditions except the P-Δ effect, with the latter not having any consequences on performance of BCJ. Thus the imposed displacements at the tip of the beam simulate the load reversal effect of the lateral drift.

Test setup comprises of mainly steel reaction frame, hydraulic jacks and supports. Steel reaction frame takes load from two hydraulic jacks, one at the top of column and the other at the beam tip. The jack at the column with loading capacity of 1200 kN is used to apply loads of different magnitude on column according to loading protocol whereas jack at the beam tip with loading

capacity of 300 kN is used to apply load reversal to simulate seismic loads. Two specially designed pin supports are also connected to the frame to support column and to allow application of loads from both the jacks. Figures 5 and 6 show the schematic diagram and BCJ test setup, respectively.

4.4 Specimens Instrumentation
Specimen instrumentation targeted the capture of all the required aspects of the experiment including the over-all structural response, local distortions, and strains in concrete and steel. Instrumentation was done in two stages. At first stage electrical strain gauges were installed on steel reinforcement before casting of concrete. Second stage instrumentation was done in laboratory, which comprised of installation of external sensors; like concrete strain gauges, LVDT's and extensometer. The test setup was also equipped with LVDT's to measure any possible over-all rigid movements of the specimen.

4.5 Loading Procedure
Four specimens with similar details were subjected to different magnitudes of axial load on column according to axial load protocol as tabulated in Table 3. Displacement controlled test was carried out and load on beam tip was applied until failure of BCJ. The range of column axial load variations from no load to 0.7 $f'_c A_g$ was considered
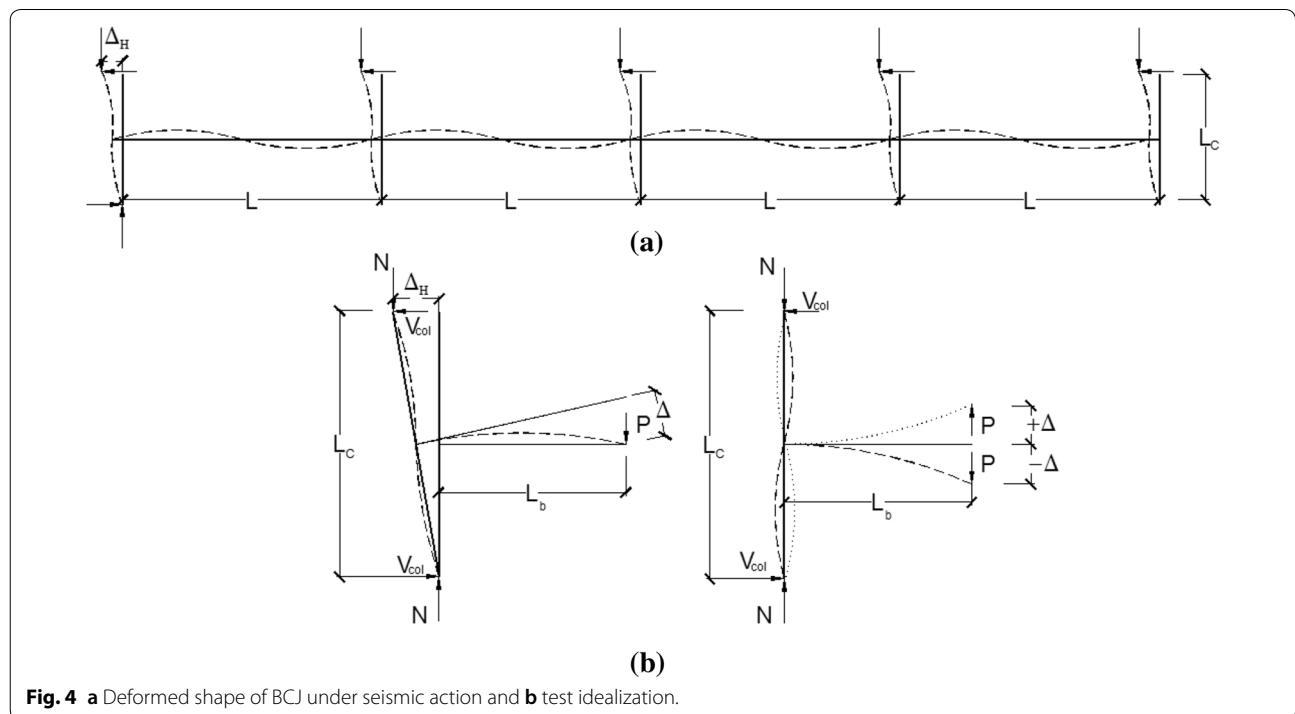

Fig. 4 **a** Deformed shape of BCJ under seismic action and **b** test idealization.

Al-Osta *et al. Int J Concr Struct Mater* (2018) 12:46
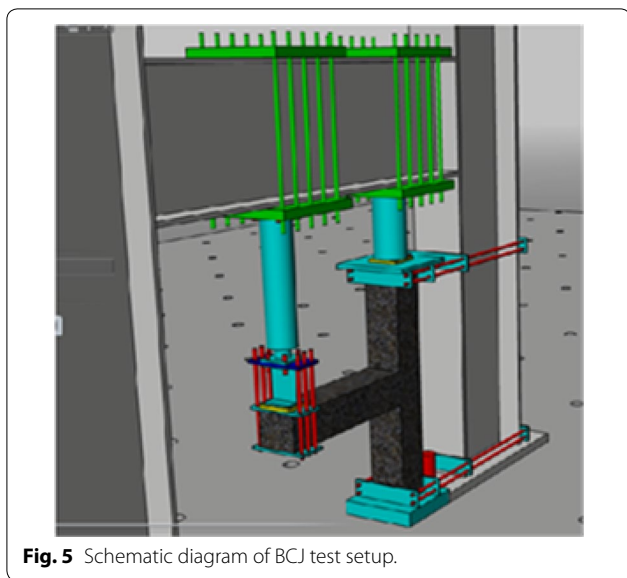
Page 6 of 20

Fig. 5 Schematic diagram of BCJ test setup.

Fig. 6 Test setup.

Table 3 Summary of loading on specimens.

Specimen ID	Magnitude of axial load (kN)	Axial load ratio (ALR), $\frac{N}{A_g f_c'}$	Test method
SP-1	0	0.00	Monotonic
SP-2	200	0.19	Monotonic
SP-3	600	0.57	Monotonic
SP-4	200	0.19	Reverse cyclic
SP-5	600	0.57	Reverse cyclic
SP-6	1050	0.70	Monotonic
SP-7	1050	0.70	Reverse cyclic

in order to capture the behavior over the entire range, both in terms of strength and failure mechanism, where A_g is the gross column cross-sectional area.

Reverse cyclic load tests were carried out on the three specimens in order to understand the performance of BCJs subjected to different magnitudes of axial and cyclic loads, simulating the actual scenario to which BCJs are subjected to under seismic excitation. In these tests, axial load of different magnitudes was applied on the column, whereas reverse cyclic load was applied at the beam tip and subsequently increased until the complete failure of BCJs according to loading protocol as shown in Fig. 7.

5 Experimental Results and Discussions
5.1 Effect of Axial Load on Shear Strength of BCJ Subjected to Monotonic Loading
Figure 8 shows the load displacement response of experimentally tested BCJs. Specimen SP-1, SP2, SP-3 and SP-6 were tested at an axial load ratio of 0.00, 0.19, 0.57 and 0.70, respectively. Continuous loading was applied at beam tip until tip displacement reached a value of 20 mm (in three of the specimens) where specimen stiffness reduced to zero. However, the softening branch was captured only in the specimens subjected to reverse cyclic loading. Increase in failure load was observed with an increase in an axial load on the column, which may be attributed to the fact that the higher axial load confined the joint against shear failure.

Figure 9 displays the crack pattern observed in specimens subjected to monotonic tests at failure load. In specimen SP 1, the first crack appeared at the center of joint which propagated towards the outer edge of column in an upward direction and towards the lower beam-joint interface in downward direction giving the inclination of the main diagonal crack at 45°. In Specimen SP-2 with increase of an ALR from 0.0 to 0.19, the crack initiation at joint was delayed i.e. first crack in the joint appeared at 29 kN as compared to Specimen SP-1 where first crack appeared at 16 kN. Inclination of main diagonal shear crack also increased to 50°. With increase of an ALR to 0.57 $f_c' A_g$ in Specimen SP-3, the crack initiation and pattern considerably changed. First crack in the joint appeared at 43 kN with inclination of around 75°. In Specimen SP-6 at ALR of 0.70 $f_c' A_g$ all the cracks that appeared in the joint were almost inclined at 90° and appeared at 45 kN. Some vertical cracks also formed on the outer face of the joint at later phases of loading. All specimens failed in joint shear failure mode since the maximum strain observed in beam longitudinal reinforcement of SP-1, SP-2, SP-3 and SP-6 was 660, 810, 990 and 1199 με, far less than the yield strain of 3100 με. It is observed that high axial load increased the inclination of main diagonal shear cracks and delayed the initiation of first shear and beam-joint interface crack.

5.2 Effect of Axial Load on Shear Strength of BCJ Subjected to Reverse Cyclic Loading
Figure 10a displays the hysteresis response of specimen SP-4. The maximum load in the positive and negative
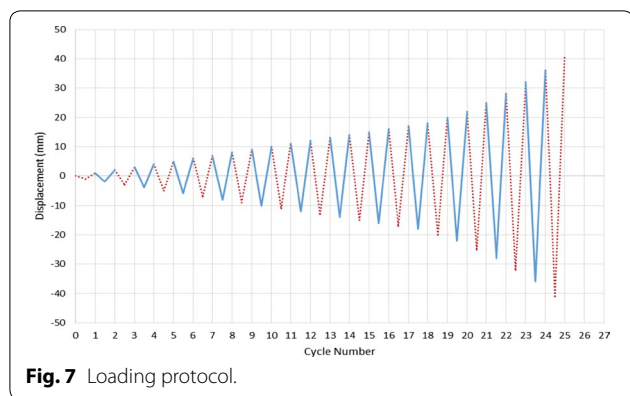
Al-Osta *et al. Int J Concr Struct Mater* (2018) 12:46

Page 7 of 20

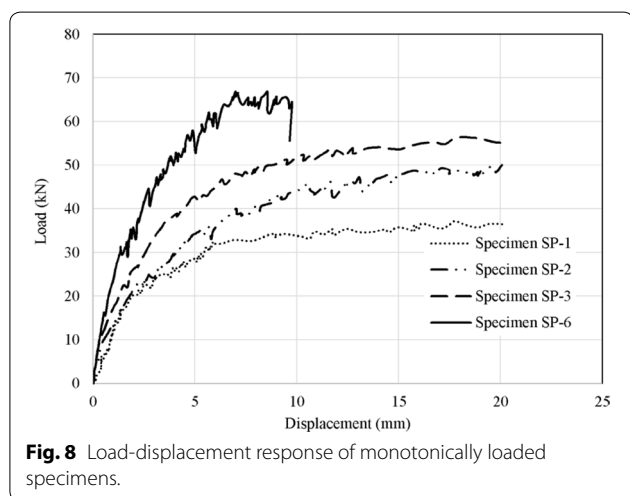**Fig. 7** Loading protocol.

Fig. 8 Load-displacement response of monotonically loaded specimens.

direction reached at 40.9 and 43 kN, corresponding to a shear strength of the joint as 2.98 and 3.09 MPa, respectively.

Pronounced pinching effect of hysteresis is observed due to formation of large number of shear cracks in the joint. The phenomenon of pinching is more prominent at high displacements due to severe shear damage of joint.

The main crack seemed right at the center of the joint at 20 and 27 kN during push and pull respectively at an inclination of 45°. After the peak load, cracks in both directions increased in width and propagated towards the column. Vertical cracks at the outer edge of joint were initiated and crack at beam-joint interface also increased excessively at later phases of loading. BCJ of specimen SP-4 failed in joint failure mode with typical wedge crack pattern as shown in Fig. 11.

Figure 10b displays the hysteresis response of specimen SP-5. The maximum load in the positive and negative direction reached 47.3 and 50.0 kN, corresponding to a shear strength of the joint as 3.43 and 3.50 MPa, respectively.

Pinching effect of hysteresis in this specimen is comparatively less as compared to specimen SP-4 which is due to the fact that high axial load confined the joint against shear failure and therefore reducing the pinching effect.

Main diagonal shear cracks appeared at the center of the joint at an inclination of around 75° at 36 and 32 kN during push and pull, respectively. With subsequent loading cycles, crack widths and length increased and several parallel cracks were observed until complete joint shear failure (Fig. 12).

Figure 10c displays the hysteresis response of specimen SP-7. The maximum load in the positive and negative direction reached 58.9 and 54.0 kN, corresponding to a shear strength of the joint as 4.58 and 4.30 MPa, respectively.

It can be noticed that pinching effect of hysteresis in this specimen is even far less as compared to specimen SP-4 and SP-5. In addition, excessive fine cracks were observed in beam of specimen SP-7 as compared to the specimens SP-4 and SP-5. Although specimen SP-7 failed in joint shear failure mode as reinforcement of both beam and column had not yielded, but slight crushing of concrete at the outer edge of joint was also observed at ultimate failure of joint.

Figure 13 shows propagation of cracks observed throughout the test. Several hair line cracks appeared in the beam in the initial loading cycles. However, the main diagonal shear cracks appeared at the middle of BCJ at 51 kN during pull and push, respectively, at an angle of around 85°. Although specimen SP-7 failed in joint shear failure mode as reinforcement of both beam and column had not yielded, but slight crushing of concrete at the outer edge of joint was also observed at ultimate failure of joint.

Figure 14 shows comparison of load–displacement response and normalized shear strength—axial load ratio (ALR) interaction curves of BCJs subjected to monotonic and reverse cyclic loading. In both the cases, increase in shear strength of BCJs is observed with increase in ALR. However, shear strength of joints subjected to reverse cyclic loading is on average 14% less as compared to their monotonic counterparts due to continuous strength degradation associated with each cycle of loading. Table 4 tabulates the results of all experimentally tested specimens.

6 Numerical Modeling of BCJs

The finite element model presented below delineates the modeling to simulate concrete followed by modeling of reinforcing steel and its bond behavior with concrete. Dynamic explicit approach was adopted to overcome convergence problems associated with softening of
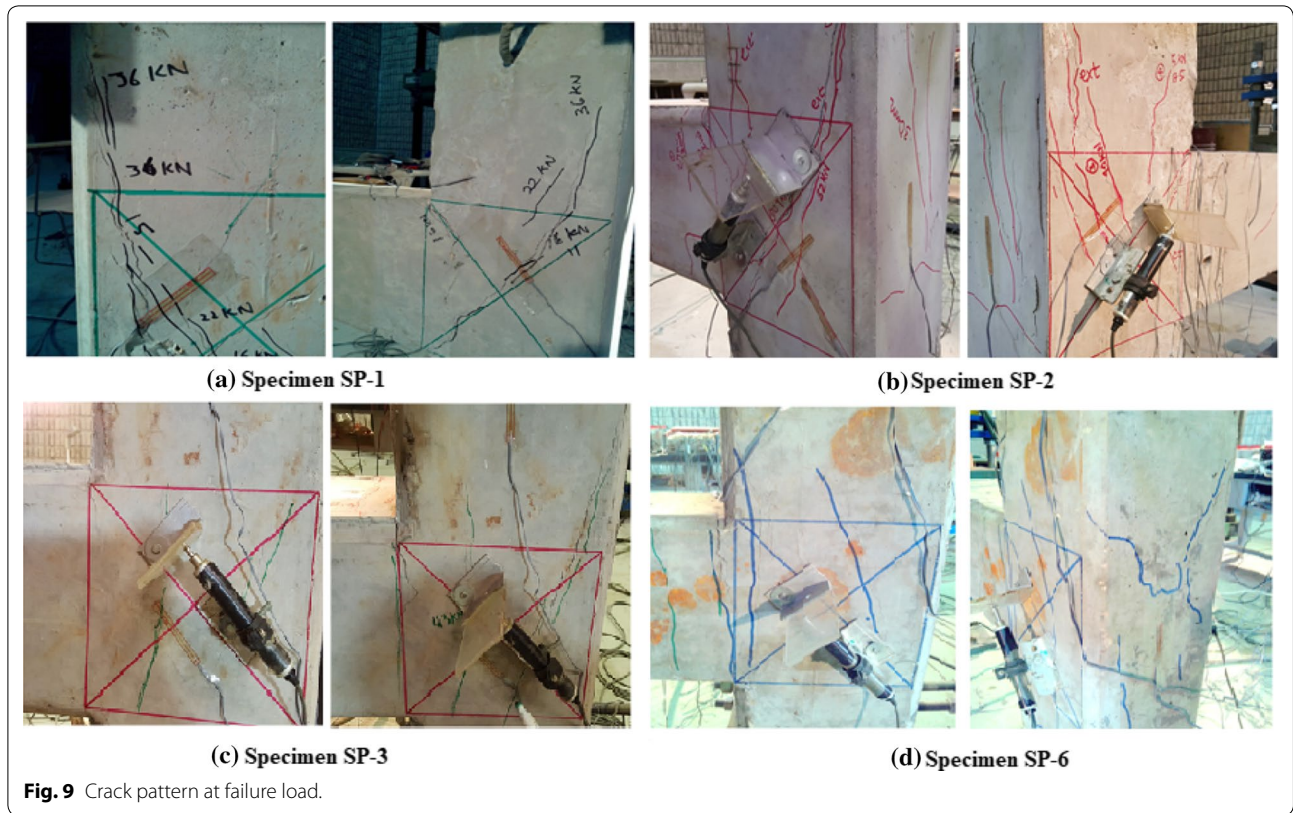
(a) Specimen SP-1　　　　　　　　　　　　　　**(b) Specimen SP-2**

(c) Specimen SP-3　　　　　　　　　　　　　　**(d) Specimen SP-6**

Fig. 9 Crack pattern at failure load.

concrete in tension. Non-linear finite element software ABAQUS was utilized to implement a finite element model as outlined in the next section.

6.1 Finite Element Model

6.1.1 Models to Simulate Cracking in Concrete

To simulate quasi-brittle nature of reinforced concrete, various conceptual models are available in the literature, which include discrete crack model, smeared crack model and concrete damage plasticity model. In this research, damage plasticity model has been utilized for concrete which is a constitutive model available in nonlinear finite element software ABAQUS. In damage plasticity model, compression and tension are two hardening variables that control the evolution of the yield surface. A continuum damage mechanics is used to model the damage by stiffness degradation approach which essentially means that the modulus of elasticity is degraded in the concrete where it cracks.

6.1.2 Modelling of Concrete

To model a concrete material in ABAQUS "concrete damaged plasticity" is used which requires the following material functions:

1. Uniaxial stress–strain relation of concrete under compressive and tensile loading.
2. Damage parameters d_c and d_t for compressive and tensile stress states, respectively.

Model Code of Fib (2010) for Concrete Structures has been adopted, as this model has advanced parameters to control ascending as well as post-peak behavior of stress–strain curve for concrete. The compressive stress–strain relationship is as follows:
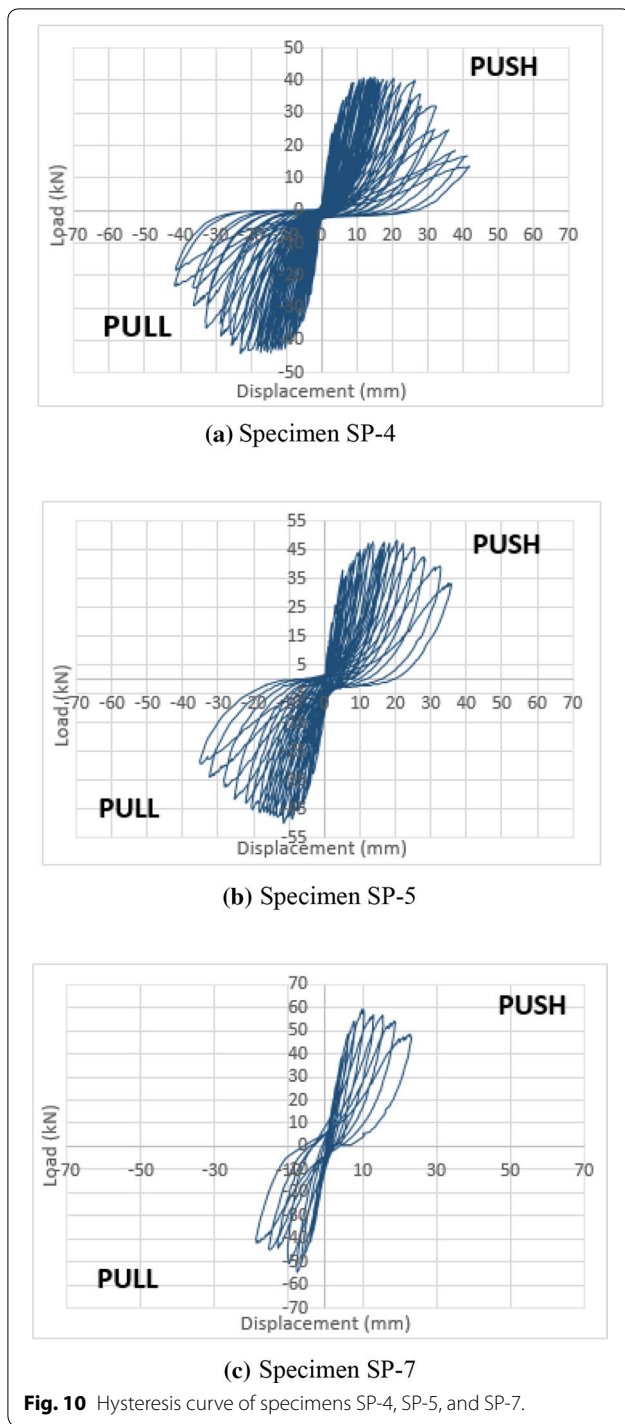
$$\frac{\sigma_c}{f_{cm}} = -\left(\frac{k \cdot \eta - \eta^2}{1 + (k-2) \cdot \eta} \right) \tag{11}$$

where: $\eta = \varepsilon_c/\varepsilon_{c1} = E_{ci}/E_{c1}$; f_{cm} is the concrete compressive strength; ε_c is the concrete compressive strain; ε_{c1} is the strain at maximum compressive stress; E_{ci} is the modulus of elasticity at 28 days; E_{c1} is the secant modulus and k is the plasticity number.

Figure 15a shows the compressive stress–strain relationship with related parameters.

Following bilinear stress strain relationship is used for tensile behavior of concrete Fig. 15b:

$$\sigma_{ct} = E_{ci}\varepsilon_{ct}\, for\, \sigma_{ct} \leq 0.9 f_{ctm} \tag{12}$$

Al-Osta *et al. Int J Concr Struct Mater* (2018) 12:46

Page 9 of 20

(a) Specimen SP-4

(b) Specimen SP-5

(c) Specimen SP-7

Fig. 10 Hysteresis curve of specimens SP-4, SP-5, and SP-7.

$$\frac{\sigma_{ct}}{f_{ctm}} = \left(1 - 0.1 \frac{0.00015 - \varepsilon_{ct}}{0.00015 - 0.9 f_{ctm}/E_{ci}}\right) for\ 0.9 f_{ctm} \leq \sigma_{ct} \leq f_{ctm}$$

(13)

Where ε_{ct} is the tensile strain; σ_{ct} is the tensile strain and f_{ctm} is the tensile strength.

Figure 15b shows the tensile stress–strain relationship with related parameters.

Concrete compression damage parameter that is used in model is given as (Birtel and Mark 2006):

$$d_c = 1 - \frac{\sigma_c E_c^{-1}}{\varepsilon_c^{pl}\left(\frac{1}{b_c} - 1\right) + \sigma_c E_c^{-1}}$$

(14)

where: d_c is concrete tension damage parameter; σ_c is compressive stress; E_c is concrete elastic modulus; $\varepsilon_c^{pl} =$ is plastic strain corresponding to compressive stress; b_c is constant with range $0 < b_c < 1$.

Whereas concrete tension damage parameter that is used in model is given as (Birtel and Mark 2006):

$$d_t = 1 - \frac{\sigma_t E_c^{-1}}{\varepsilon_t^{pl}\left(\frac{1}{b_t} - 1\right) + \sigma_t E_c^{-1}}$$

(15)

where: d_t is concrete tension damage parameter; σ_t is tensile stress; $\varepsilon_t^{pl} =$ is plastic strain corresponding to tensile stress; b_t is constant with range $0 < b_t < 1$.

The concrete parameters used in the plastic damage model are shown in Table 5.

6.1.3 Modelling of Reinforcing Steel and its Bond with Concrete

Reinforcing steel has been modelled using truss element in ABAQUS. The stress–strain curve for steel obtained through experiment is shown in Fig. 16. The other parameters used to define reinforcing steel are shown in Table 6.

Steel reinforcement is bonded with concrete as an embedded element in ABAQUS. Embedment technique allows number of elements to be embedded inside another element known as host element. Thus, modeling of interaction surface between the embedded and the host element is not required, which eradicates numerically costly iterations linked with surface formulations. Essentially, perfect bond is assumed between concrete and the reinforcement in this model, as there was no experimental evidence of any bond slip during the testing of the specimens.

6.2 Validation of Finite Element Model

The FE model described above has been validated with experimental results. A comparison of experimental results and FE model prediction is presented next to validate its competency to envisage the failure load, mode of failure and overall behavior of BCJs.

6.2.1 Specimen SP-1

Load displacement response predicted by FEM for specimen SP-1 is shown in Fig. 17a along with experimentally
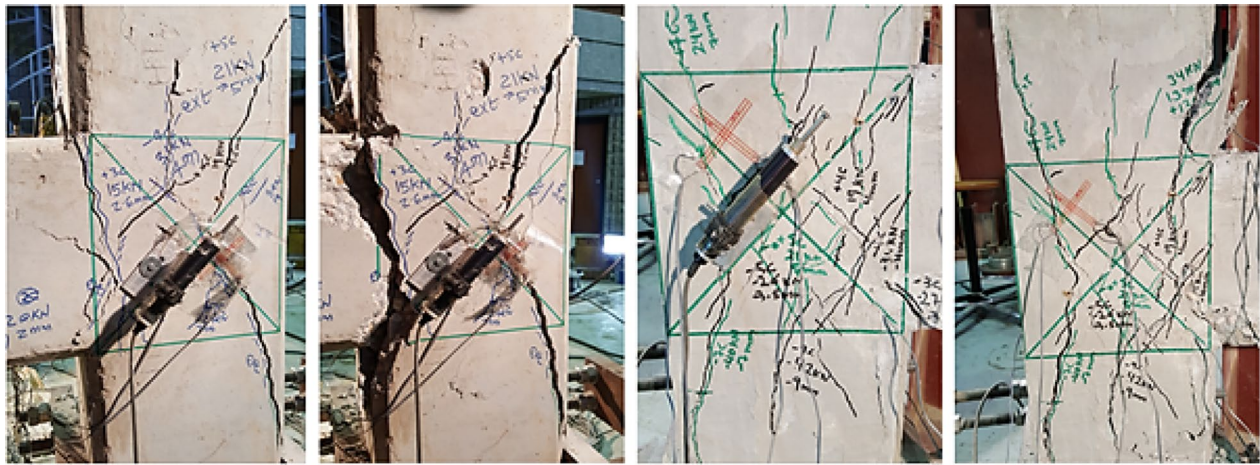
Al-Osta *et al. Int J Concr Struct Mater* (2018) 12:46

Page 10 of 20

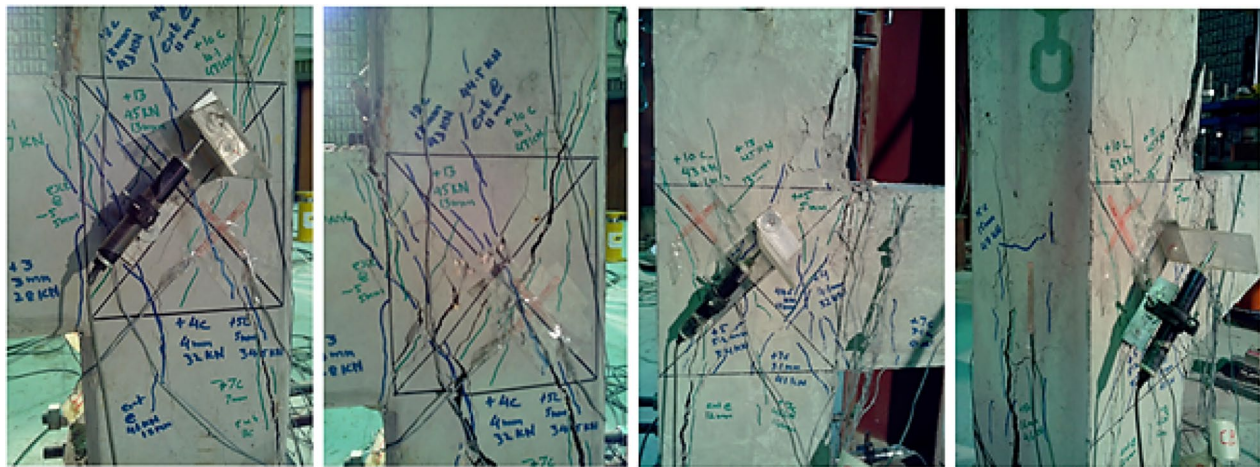**Fig. 11** Crack pattern at intermediate and final loading stage of specimen SP-4.

**Fig. 12** Crack pattern at intermediate and final loading stage of specimen SP-5.

obtained curve. Maximum load at beam predicted by FEM is 36.11 kN at displacement of 18.34 mm against experimental value of 37.55 kN at displacement of 19.44 mm. Overall FEM prediction of load displacement response matches well with that of the experiment. The predicted failure mode of specimen SP-1 is joint failure mode as expected from the results of experiment. The crack pattern of the experiment and FE prediction based on values of damage parameter d_t is also well matched as shown in Fig. 18a. Figure 19a shows the steel strains at failure load of specimen SP-1. The average maximum strain in beam's top longitudinal bars is obtained as 0.000687 mm/mm which is in good agreement with the experimental value of 0.00066 mm/mm. The joint shear stress calculated with FEM results is 2.77 MPa against 2.74 MPa as determined experimentally.
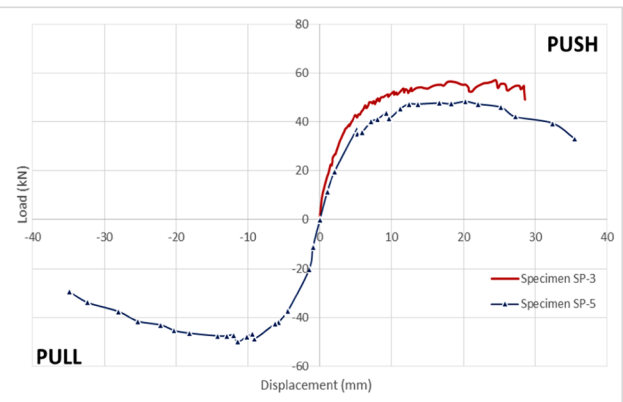
6.2.2 Specimen SP-2
Figure 17b shows the load–displacement response of specimen SP-2 obtained experimentally and as predicted by FEM. Failure load predicted by FEM is 50.13 kN corresponding to displacement of 16.75 mm against experimental value of 50.08 kN at a displacement of 19.48 mm. In general, the load displacement curve predicted by FEM is in good agreement with that obtained from the experiment. Crack pattern of the experiment and FE prediction is also well matched as shown in Fig. 18b. The predicted failure mode of specimen SP-2 is joint shear failure mode. Figure 19b shows the steel strains at failure load of specimen SP-2. The average maximum strain in beam's top bars is obtained as 0.00096 mm/mm against experimental value of 0.00088 mm/mm. The joint shear
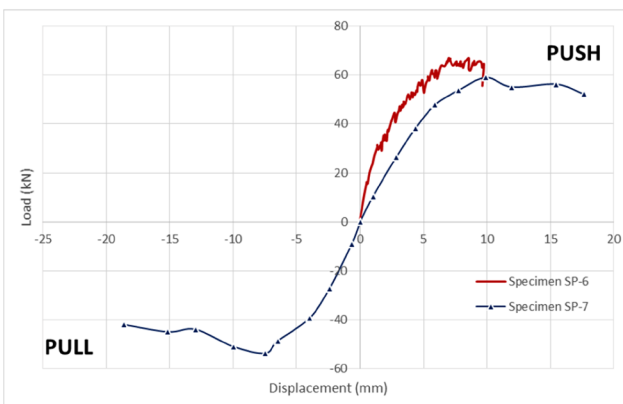
Al-Osta *et al. Int J Concr Struct Mater* (2018) 12:46

Page 11 of 20

Fig. 13 Crack pattern at intermediate and final loading stage of specimen SP-7.
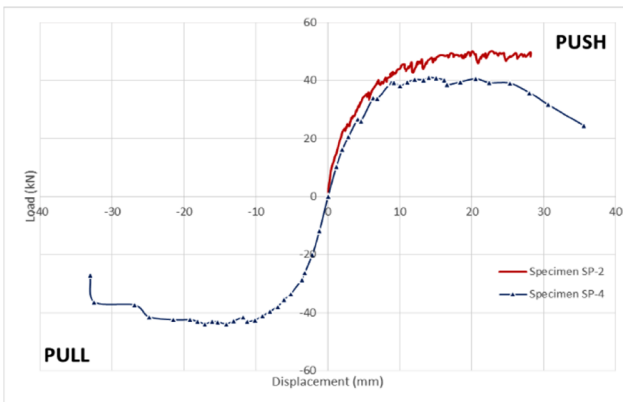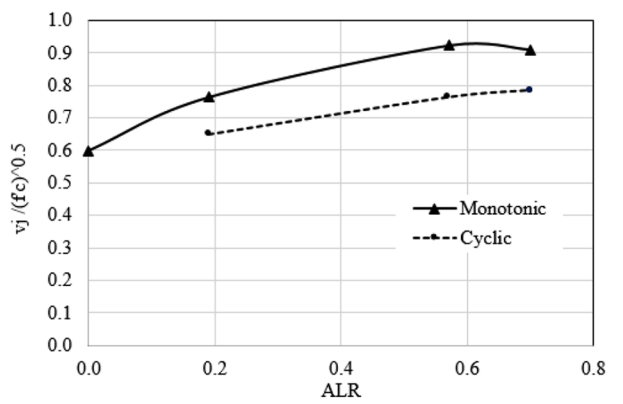

(a) Specimen SP-2 and SP-4

(b) Specimen SP-3 and SP-5

(c) Specimen SP-6 and SP-7

(d) Normalized shear strength-ALR interaction

Fig. 14 Comparison of load–displacement response and normalized shear strength-ALR interaction curves.

Al-Osta *et al. Int J Concr Struct Mater* (2018) 12:46

Page 12 of 20

Table 4 Results summary of test specimens.

Specimen ID	Load	σ_N (f'c %)	ICL (kN)	JCL (kN)	P (kN)	T (kN)	$V_{u(col)}$ (kN)	$V_{j(Joint)}$ (kN)	$v_{j(Joint)}$ (MPa)
SP-1	M	0.00	16	16	37	166	28	137	2.74
SP-2	M	0.19	29	29	51	212	37	174	3.50
SP-3	M	0.57	38	38	57	254	43	211	4.23
SP-6	M	0.70	45	45	66	310	49	260	5.20
SP-4	RC	0.19	20	21	41/43	182/187	31/32	152/155	2.98/3.09
SP-5	RC	0.57	27	36	47/50	207/210	35/37	171/172	3.43/3.50
SP-7	RC	0.70	51	51	59/54	273/255	44/40	228/215	4.58/4.30

M Monotonic; *RC* reverse cyclic; *ICL* beam-joint interface cracking load; *JCL* joint cracking load; *P* beam tip load; *T* tension force in beam reinforcement; $V_{u(Joint)}$ is the column shear; $V_{j(Joint)}$ is the joint shear force; $v_{j(Joint)}$ is equivalent joint shear strength.
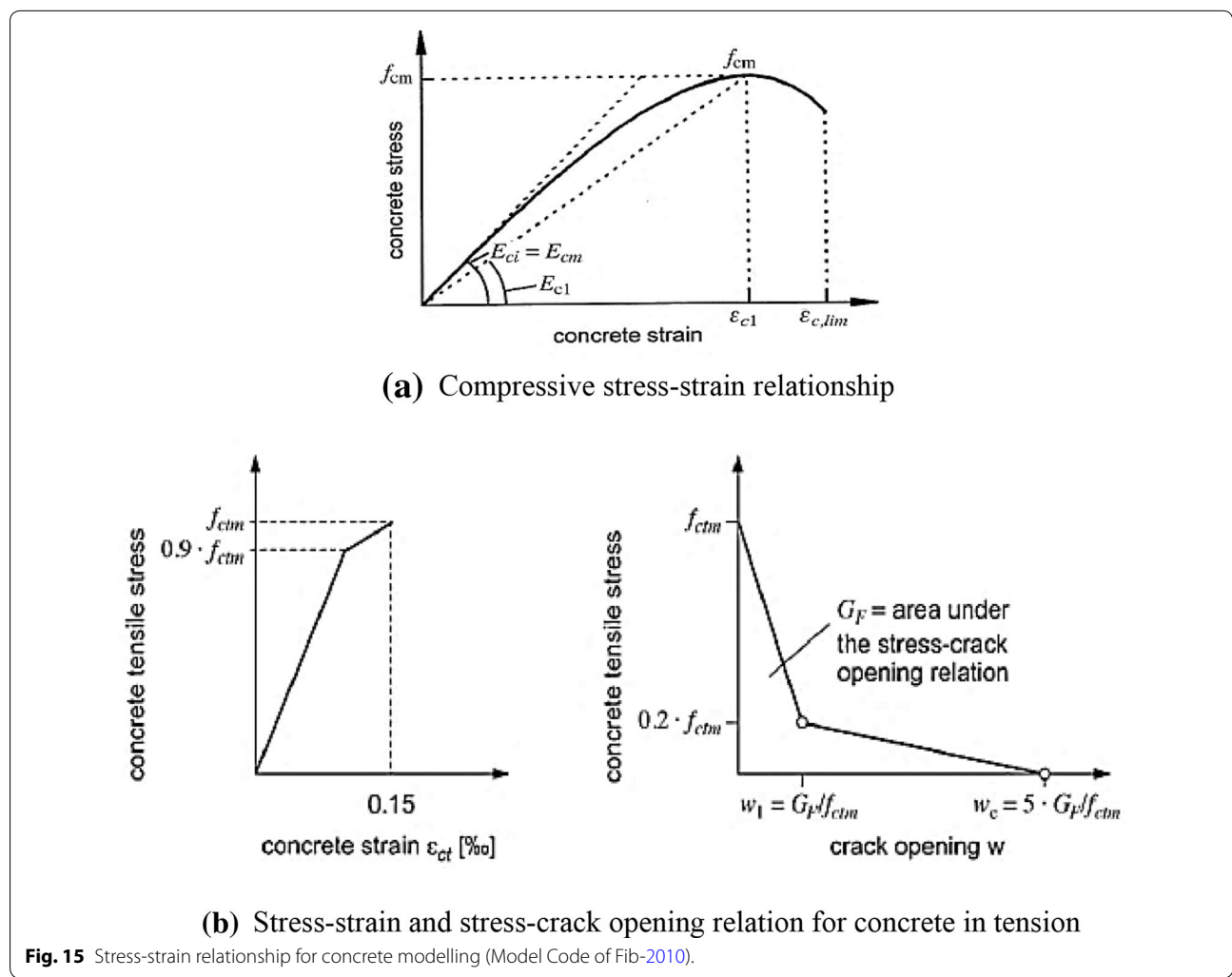

(a) Compressive stress-strain relationship

(b) Stress-strain and stress-crack opening relation for concrete in tension

Fig. 15 Stress-strain relationship for concrete modelling (Model Code of Fib-2010).

Table 5 Concrete parameters used in the plastic damage model.

Concrete strength (MPa)	Mass density (tonne/mm³)	Young's modulus (MPa)	Poisson's ratio	Dilation angle Ψ (degrees)	Plastic potential eccentricity ϵ	f_{bo}/f_{co}	b_c/b_t
Varies	2.4E−009	Varies[a]	0.19–0.20	36	0.1	1.16	0.7

[a] As per concrete strength (21, 30, 36, 50, 65 MPa).

Al-Osta *et al. Int J Concr Struct Mater (2018) 12:46*

Page 13 of 20

Fig. 16 Stress-strain curve of reinforcing steel.
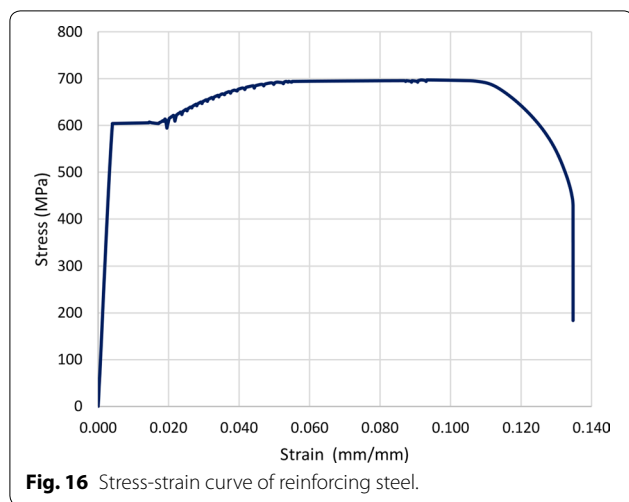
Table 6 Parameters used to define reinforcing steel.

Elastic modulus (MPa)	193600/195161
Poisson's ratio	0.3
Mass density (tonne/mm^3)	7.85E−009
Yield stress (MPa)	580/605

stress predicted by FEM is 3.71 MPa in comparison to experimental value of 3.45 MPa.

6.2.3 Specimen SP-3

Failure load predicted by FEM is 58.78 kN corresponding to displacement of 18.23 mm against experimental value of 56.87 kN at a displacement of 17.86 mm. In general, the load displacement curve predicted by FEM is in good agreement with that obtained from the experiment as shown in Fig. 17c. The predicted failure mode of observed is joint failure and the crack pattern of the experiment and FE prediction is shown in Fig. 18c where cracks are at greater inclination than the previous two cases. Figure 19c shows the steel strains at failure load of specimen SP-3. The average maximum strain in beam's top bars is obtained as 0.00106 mm/mm against experimental value of 0.00098 mm/mm. The joint shear stress predicted by FEM is 4.43 MPa in contrast to the experimental value of 4.23 MPa.

6.2.4 Specimen SP-6

Failure load predicted by FEM is 68.66 kN corresponding to displacement of 5.81 mm against experimental value of 66.94 kN at a displacement of 6.98 mm. In general, the load displacement curve predicted by FEM is in close agreement with that of the experiment as shown in

Fig. 17d. The predicted failure mode of specimen SP-6 is joint shear failure. The crack pattern of the experiment and FE prediction is shown in Fig. 18d where joint shear cracks are almost vertical. Figure 19d shows the steel strains at failure load of specimen SP-6. The average maximum strain in beam's top longitudinal bars is obtained as 0.00127 mm/mm which closely matches with the experimental value of 0.00119 mm/mm. The shear stress calculated with FEM results is 5.36 MPa against 5.06 MPa as obtained experimentally.

6.3 Parametric Study Using Finite Element Modeling

Based on validation of FE model using experimental results as discussed in the previous section, the calibrated FE model is used to extend the research work for different concrete strengths in order to acquire sufficient data corresponding to various concrete strengths and levels of column axial load.

Table 7 shows the layout of the various finite element models investigated under the parametric paradigm.

BCJs with five different concrete strengths have been examined for the influence of column axial load on shear strength. Almost similar trend is observed in all the groups where shear strength increases up to ALR of 0.60–0.70 due to confinement provided by axial load to the joint against shear failure. At ALR of 0.60–0.70, small crushing in joint is observed at failure load but primarily the joint failed in joint shear failure mode up to this ALR level as no reinforcement yielding was observed, neither in the beam nor in the column. However, above ALR of 0.60–0.70, decrease in shear strength was observed in all the groups where joint failed in shear followed by axial failure mode caused by the joint axial strain exceeding the threshold limit of 4000 µε along with crushing of concrete in the joint. In all the cases, decrease in ductility was observed with increase in axial load on the column and softening started earlier for higher strength concretes. Figure 20 summarizes load–displacement whereas Fig. 21 summarizes the shear strength- axial stress relation of all the groups discussed above.

7 Shear Strength Equation for BCJs

7.1 Development of Shear Strength Equation

Figure 22 shows the comparison of mechanistic model (Sect. 3) prediction for shear strength of BCJs with results obtained from experiment and FE modeling. It can be observed that mechanistic model reasonably predicts the overall trend of shear strength over the complete range of ALR. However, due to contribution of beam reinforcement in arresting shear crack development in the joint, actual shear strength values were found to be higher over entire range of ALR. In addition,
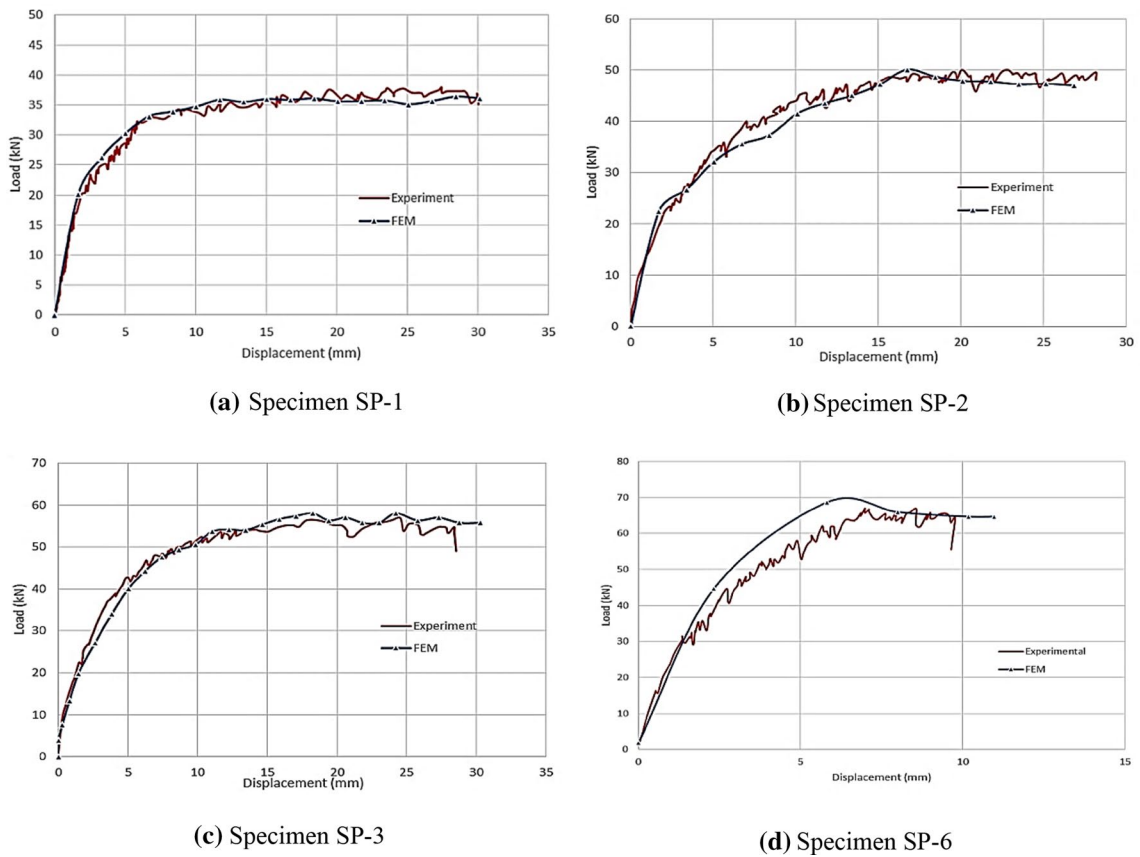
Al-Osta *et al. Int J Concr Struct Mater* (2018) 12:46

Page 14 of 20

Fig. 17 Load versus displacement response of specimens SP-1, SP-2, SP-3, and SP-6.

Fig. 18 FEM and experimental crack pattern of specimens SP-1, SP-2, SP-3, and SP-6.

Al-Osta *et al. Int J Concr Struct Mater* (2018) 12:46

Page 15 of 20

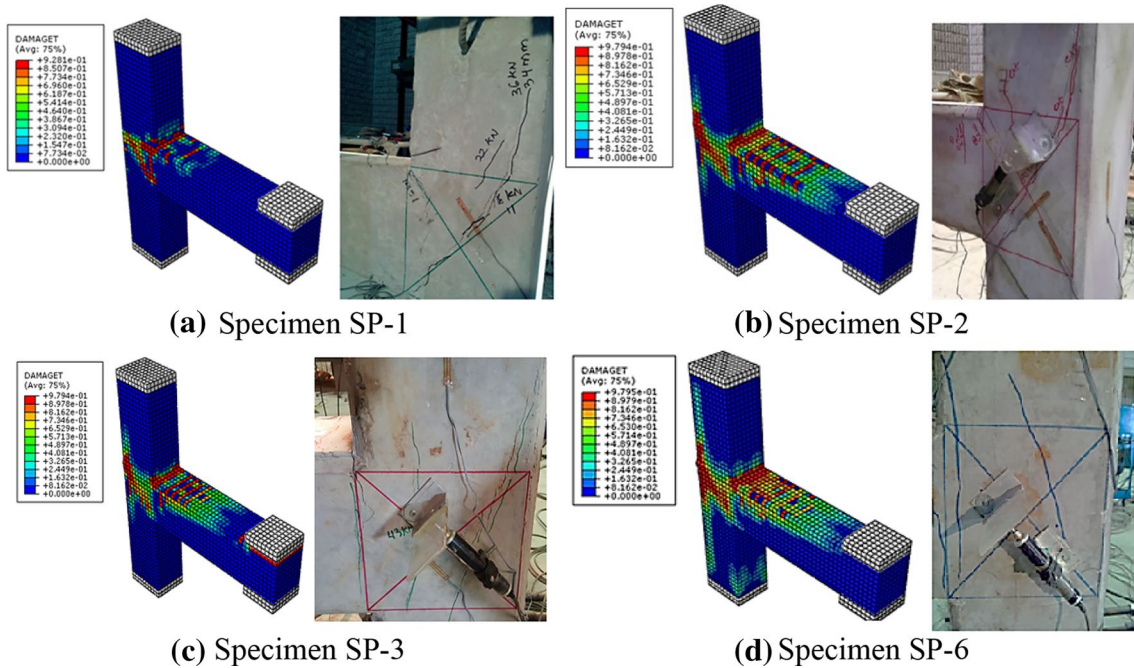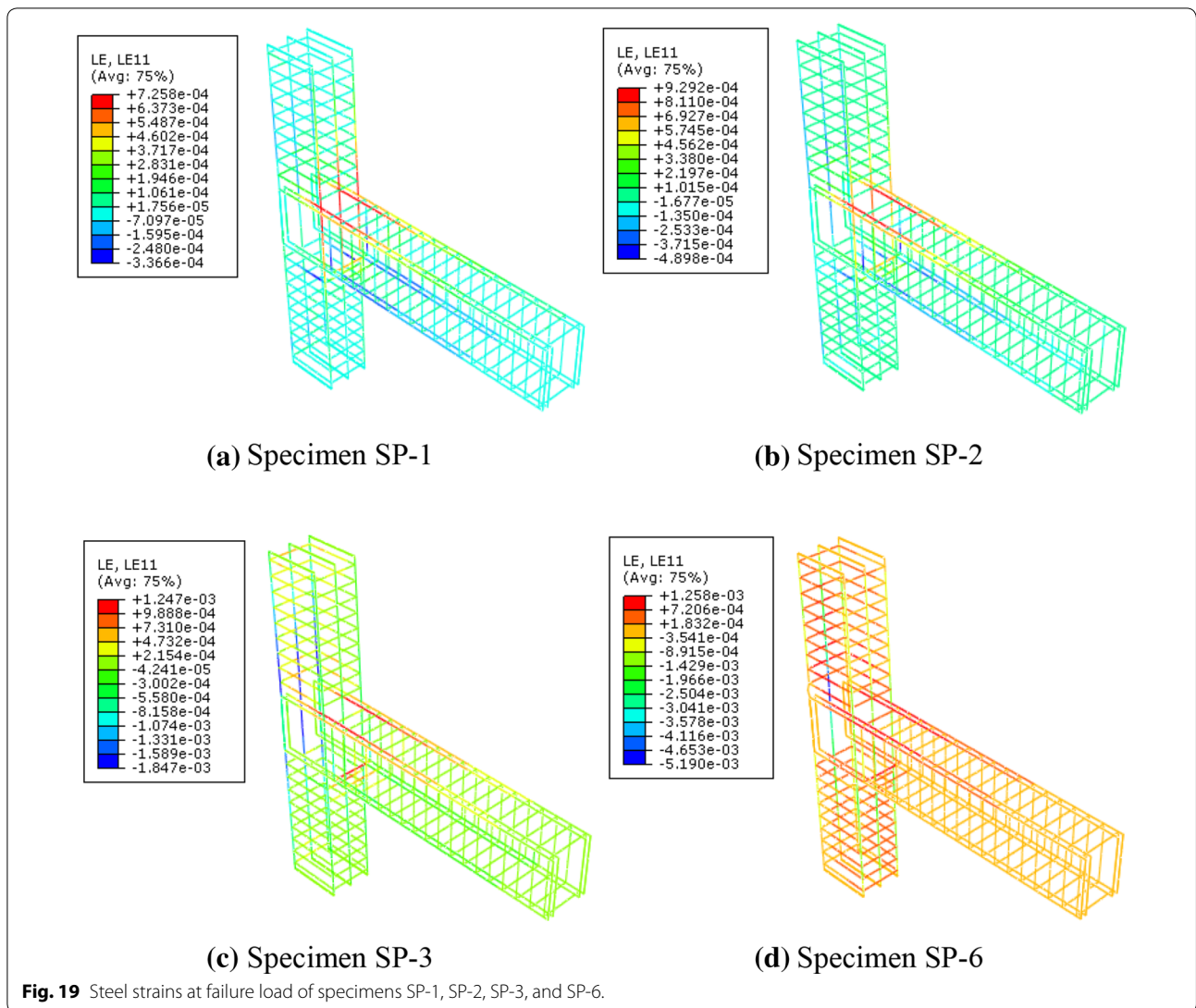**Fig. 19** Steel strains at failure load of specimens SP-1, SP-2, SP-3, and SP-6.

after a certain percentage of axial loads, unconfined joints experienced mixed states of failure i.e. shear failure and local crushing. The mechanistic model gives the maximum shear strength due to increase in axial load at around $0.45\ f_c'A_g$–$0.50\ f_c'A_g$. However, in practice, presence of column reinforcement increased the axial capacity of joint, which delayed this type of failure. This is the reason that difference in actual shear strength values and that predicted by mechanistic model was more pronounced in range of $0.50\ f_c'A_g$–$0.70\ f_c'A_g$.

Therefore, interactions between axial stress on column and corresponding shear strength of BCJs obtained from experimental and FE modeling is used to develop shear strength equations. The effects of aspect ratio and beam reinforcement are evaluated independently.

It is evident from the experiment that the beam reinforcement in the joint region increases its shear capacity

as it arrests the development of shear cracks. To evaluate the possible influence of different beam reinforcement ratio on joint shear strength, experimental test results of Hakuto et al. (2000), Ghobarah and Said (2001), Pantelides et al. (2002) and Pantelides et al. (2008) were investigated. Only those experimental tests are considered in which the aspect ratio and column axial load are almost similar in order to minimize the interaction of these parameters. Experimental shear strength was then normalized with square root of concrete compressive strength and plotted against respective beam reinforcement ratio as shown in Fig. 23. The following relation between beam reinforcement ratio ρ_b and shear strength is derived from the observed trend:

$$\frac{v_j}{\sqrt{f_c'}} = 0.7675\rho_b^{0.261} \tag{16}$$

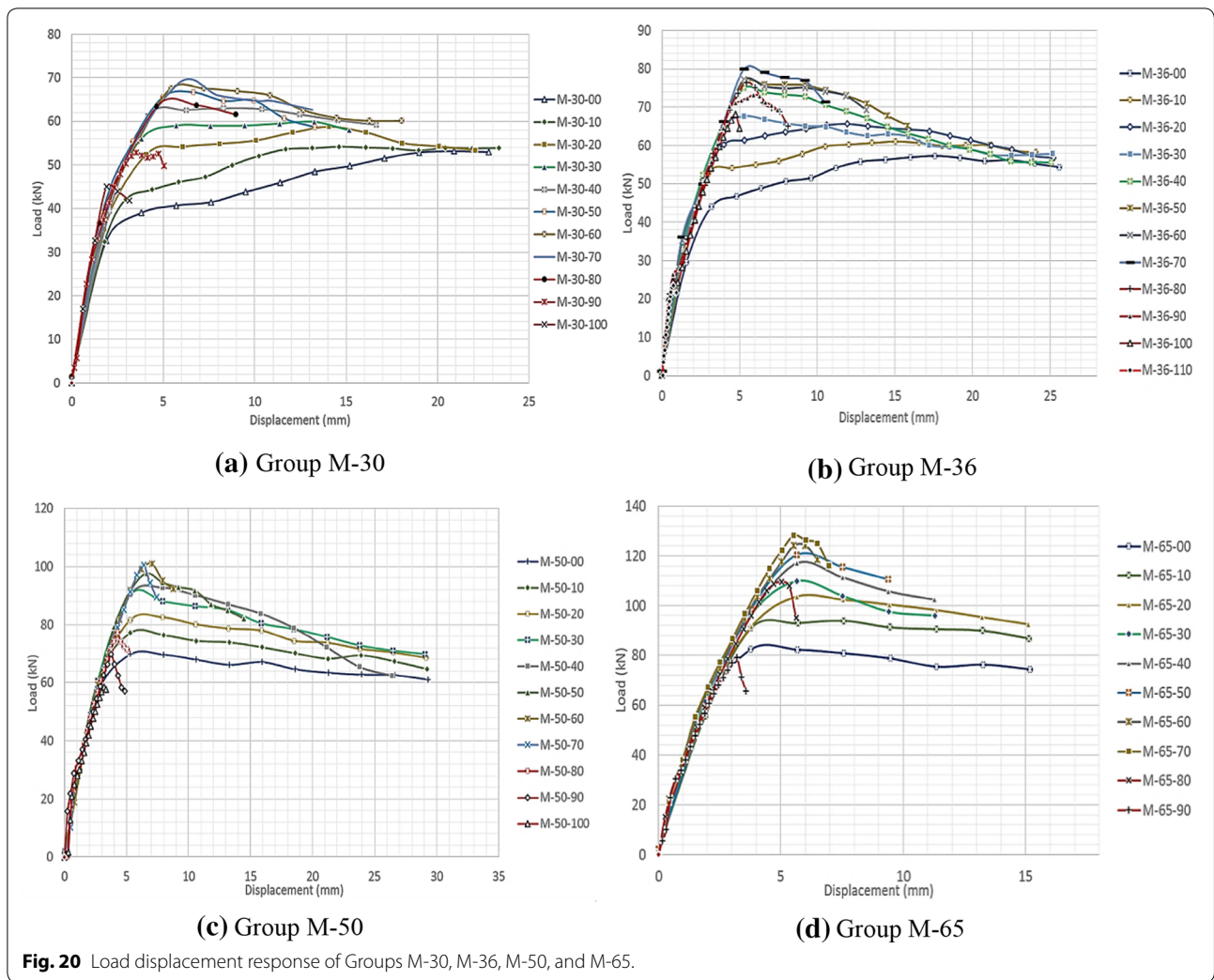Al-Osta *et al. Int J Concr Struct Mater* (2018) 12:46

Page 16 of 20

Fig. 20 Load displacement response of Groups M-30, M-36, M-50, and M-65.

To evaluate an effect of aspect ratio on shear strength of BCJ experimental results of Wong (2005), Antonopoulos and Triantafillou (2003), Pantelides et al. (2008) were investigated to cover a range of aspect ratio from 1 to 2. Those experimental results have been considered in which axial load ratio was almost similar. Shear strength was then normalized with square root of concrete compressive strength and effect of beam longitudinal reinforcement i.e. $\rho_b^{0.261}$. Normalized shear strength is then plotted against respective values of aspect ratio as shown in Fig. 24. The following relation between aspect ratio of BCJ (h_b/h_c) and shear strength is derived from the trend:

$$\frac{v_j}{\sqrt{f'_c}\rho_b^{0.261}} = 0.7543\left(\frac{h_b}{h_c}\right)^{-0.279} \tag{17}$$

7.2 Proposed Shear Strength Equation for BCJs
Effect of all the parameters affecting shear strength of unconfined joints with joint shear failure mode that include axial load on column, concrete compressive strength, beam reinforcement ratio and BCJ aspect ratio are conjoined into the following Eq. (18).

$$V_n = 0.58\sqrt{f'_c}\left(\alpha + \beta\frac{N}{A_g}\right)^y\left(\frac{A_{sb}}{b_b d}\right)^{0.261}\left(\frac{h_b}{h_c}\right)^{-0.279}\left(\frac{b_b + b_c}{2}\right)h_c \tag{18}$$

where V_n is the shear strength of joint without stirrups in Newton (N); α, β and γ are shear co-efficient tabulated in Table 8 for various ranges of ALR. N is the column axial load (N); A_g is the cross-sectional area of column at the joint (mm²); A_{sb} is area of beam reinforcement (mm²); b_b, d and h_b are the width, depth and section depth of the beam respectively (mm); b_c and h_c are the column section width and depth respectively (mm). f'_c is the concrete cylinder strength of concrete (MPa).

Al-Osta *et al. Int J Concr Struct Mater (2018) 12:46*

Page 17 of 20

Table 7 Layout of finite element models.

Group	M-21	M-30	M-36	M-50	M-65
f'c	21	30	36	50	65
ALR					
0.00	M-21-00	M-30-00	M-36-00	M-50-00	M-65-00
0.10	–	M-30-10	M-36-10	M-50-10	M-65-10
0.20	M-21-19	M-30-20	M-36-20	M-50-20	M-65-20
0.30	–	M-30-30	M-36-30	M-50-30	M-65-30
0.40	–	M-30-40	M-36-40	M-50-40	M-65-40
0.50	–	M-30-50	M-36-50	M-50-50	M-65-50
0.60	M-21-57	M-30-60	M-36-60	M-50-60	M-65-60
0.70	–	M-30-70	M-36-70	M-50-70	M-65-70
0.80	M-21-80	M-30-80	M-36-80	M-50-80	M-65-80
0.90	–	M-30-90	M-36-90	M-50-90	M-65-90
1.00	–	M-30-100	M-36-100	M-50-100	–
1.05	–	–	–	–	M-65-AC
1.08	–	–	–	M-50-AC	–
1.10	M-21-AC	M-30-AC	M-36-110	–	–
1.13	–	–	M-36-AC	–	–

Axial load ratio (ALR) $= \frac{N}{A_g f'_c}$; $f'_c =$ concrete compressive strength (MPa).
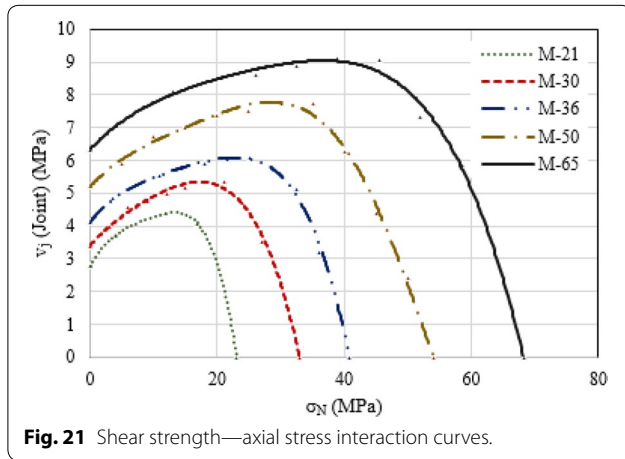

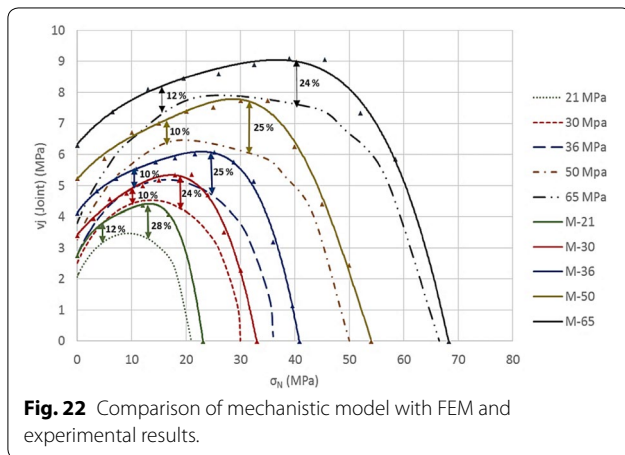**Fig. 21** Shear strength—axial stress interaction curves.

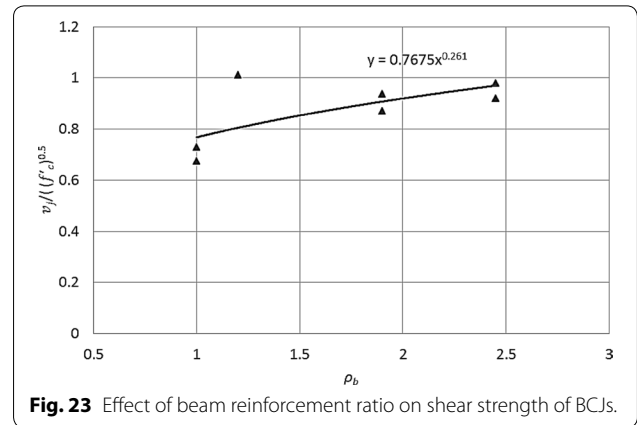**Fig. 22** Comparison of mechanistic model with FEM and experimental results.

Fig. 23 Effect of beam reinforcement ratio on shear strength of BCJs.
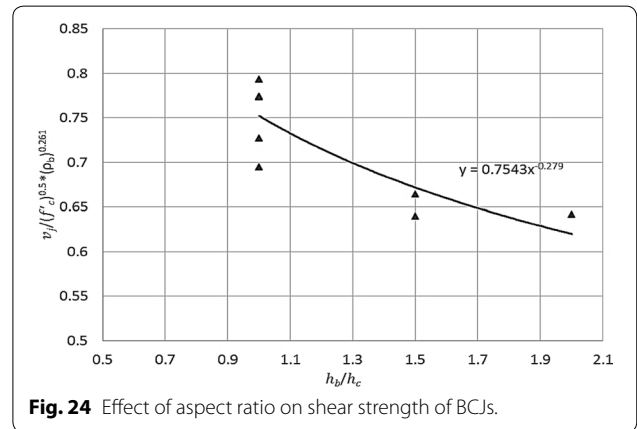

Fig. 24 Effect of aspect ratio on shear strength of BCJs.

Table 8 Values of joint shear co-efficient.

Axial load ratio $\frac{N}{A_g f'_c}$	Shear co-efficient		
	α	β	γ
0.00 < ALR ≤ 0.50	351	100	0.21
0.50 < ALR ≤ 0.70	4	0.03	1
0.70 < ALR ≤ 0.90	425	− 5	0.25

7.3 Validation of Shear Strength Equation

Database utilized to validate proposed shear strength equation is based on experimental results available in literature. In these experiments, BCJs were unconfined, longitudinal reinforcement has standard 90° hook and failure mechanism is joint shear failure mode. The maximum ALR considered in database is 0.25 due to non-availability of test results for unconfined joints with joint shear failure mode above this range. In addition, the maximum concrete compressive strength considered is

Al-Osta *et al. Int J Concr Struct Mater* (2018) 12:46

Page 18 of 20

Table 9 Validation of proposed shear strength equation.

Researchers	Specimens	Joint type	Joint aspect ratio	f'_c (MPa)	Beam ρ_{bb} (%)	ρ_{tb} (%)	f_{yb} (MPa)	Axial load ratio (ALR)	V_{Test} (MPa)	$V_{Predicted}$ (MPa)	$\frac{V_{Predicted}}{V_{Test}}$
Hakuto et al. (2000)	06	Exterior	1.1	31	0.66	1	308	0	3.75	3.23	0.86
	07	Exterior	1.1	31	0.66	1	308	0	4.05	3.23	0.80
Clyde et al. (2000)	SP 2	Exterior	0.89	46.2	2.45	2.45	454	0.10	6.26	6.31	1.01
	SP 6	Exterior	0.89	40.9	2.45	2.45	454	0.10	6.26	5.85	0.93
	SP 4	Exterior	0.89	37.0	2.45	2.45	454	0.25	7.07	6.20	0.88
	SP 5	Exterior	0.89	40.1	2.45	2.45	454	0.25	6.83	6.54	0.96
Pantelides et al. (2008)	SP 1	Exterior	1.00	33.0	1.90	1.90	459	0.10	5.39	4.65	0.86
	SP 2	Exterior	1.00	33.0	1.90	1.90	459	0.25	5.24	5.22	0.99
	SP 3	Exterior	1.00	34.0	1.90	1.90	459	0.10	5.08	4.74	0.93
	SP 4	Exterior	1.00	34.0	1.90	1.90	459	0.25	5.66	5.32	0.94
	SP 5	Exterior	1.00	31.6	1.90	1.90	459	0.10	5.46	4.53	0.83
	SP 6	Exterior	1.00	31.6	1.90	1.90	459	0.25	5.46	5.07	0.93
Wong (2005)	BS-L	Exterior	1.50	30.8	0.94	0.94	520	0.15	4.05	3.47	0.86
	BS-U	Exterior	1.50	30.9	0.94	0.94	520	0.15	4.06	3.47	0.86
	BS-LL	Exterior	1.50	42.1	0.94	0.94	520	0.15	5.39	4.22	0.78
	BS-L-LS	Exterior	1.50	31.6	0.94	0.94	520	0.15	5.06	3.52	0.70
	BS-V2T10	Exterior	1.50	32.6	0.94	0.94	520	0.15	3.19	3.59	1.13
	BS-V4T10	Exterior	1.50	28.3	0.94	0.94	520	0.15	4.76	3.29	0.69
	BS-L600	Exterior	2.00	36.4	0.68	0.68	520	0.15	3.38	3.26	0.97
Ghobarah and Said (2001)	T 1	Exterior	1.00	30.9	1.20	1.20	425	0.19	5.58	4.27	0.77
	T 2	Exterior	1.00	30.9	1.20	1.20	425	0.10	5.63	3.97	0.70
Antonopoulos and Triantafillou (2003)	C1	Exterior	1.50	19.4	0.77	0.77	585	0.05	2.57	2.30	0.90
	C2	Exterior	1.50	23.7	0.77	0.77	585	0.05	2.95	2.57	0.87

Average = 0.88
Standard deviation = 0.10

Axial load ratio (ALR) $= \frac{N}{A_g f'_c}$; f'_c concrete compressive strength; ρ_{bb} beam bottom reinforcement percentage; ρ_{tb} beam top reinforcement percentage; f_{yb} beam reinforcement yield strength; Aspect ratio $= \frac{beam\,depth}{Column\,depth}$; N column axial load; V_{Test} shear strength from experiment; $V_{Predicted}$ shear strength predicted by proposed equation.

Al-Osta *et al. Int J Concr Struct Mater* (2018) 12:46

Page 19 of 20

46.2 MPa. Table 9 tabulates the validation of proposed shear strength equation.

7.4 Discussion on Proposed and Previous Shear Strength Equations

Several shear strength equations available in literature including present design guidelines are deficient in predicting shear strength of unconfined joints in one or another way. For example Vollum and Newman (1999) model considered the effect of aspect ratio and f'_c but did not account for the important influencing parameters such as column axial load and beam reinforcement ratio. Bakir and Boduroglu (2002) considered the effect of beam reinforcement ratio, aspect ratio and f'_c but did not account for the column axial load which is a key influencing parameter in determining joint shear strength. Sarsam and Phillips (1985) considered the effect of aspect ratio of joint, column reinforcement ratio and axial load on column up to ALR of 0.42 but did not include the effect of beam reinforcement ratio. Current design guidelines of ACI-ASCE Committee 352 (2002) at first assumes that tension steel yields and further, these guidelines do not take into account key parameters like aspect ratio, beam reinforcement ratio and column axial load in estimating shear strength of joint. The shear strength model proposed in this work considers all the effects including column axial load, concrete compressive strength, joint aspect ratio and beam reinforcement ratio and has been validated with experimental database of unconfined joints, giving an average of $V_{Predicted}/V_{Test}$ of 0.88 with standard deviation of 0.10 as compared to $V_{ACI}/V_{Test} = 0.64$ with standard deviation of 0.32. Thus, it is concluded that proposed shear strength equation gives representative and conservative estimates of joint shear strength.

8 Conclusions

Based on extensive results of the experimental and numerical work carried out and documented in this research, following important conclusions may be drawn:

1. Increasing the column axial load from zero to 0.60 $f'_c A_g$ enhances the shear strength of BCJ by 42% of the joint strength at zero axial load.
2. Shear strength of joint in range of column axial load from 0.60 $f'_c A_g$ to 0.70 $f'_c A_g$ was found to be almost invariant.
3. Increase in column axial load above a level of 0.70 $f'_c A_g$ was found to decrease the shear strength of joint rapidly, leading to a failure of the joint driven purely by the column axial load at magnitude of 1.00 $f'_c A_g$–1.10 $f'_c A_g$.

4. High column axial load was noted to increase the inclination of joint shear cracks at failure. Such increase in crack orientation matches those predicted by traditional concrete failure theories such as Mohr–Coulomb.
5. An average reduction in shear strength of BCJ due to reverse cyclic loading was found to be around 14% as compared to its monotonic loading counterpart.
6. High axial load was noted to delay the initiation of first shear and beam-joint interface crack.
7. Ductility of BCJ was found to reduce with an increase in axial load on column. This effect was more pronounced for column axial loads of 0.60 $f'_c A_g$ and greater.
8. Above column axial load of 0.60 $f'_c A_g$, the rate of stiffness degradation was found to increase drastically due to greater deterioration caused by local crushing.
9. The proposed shear strength equation has taken into account the influence of important variables including the effect of column axial load, concrete compressive strength, joint aspect ratio and beam reinforcement ratio in predicting the joint shear strength.
10. It is found that the proposed shear strength model is capable of predicting results from several other research contributions, including the influence of column axial load magnitude and other important variables. Therefore, it is believed that the proposed model gives representative and conservative estimates of joint shear strength for unconfined joints.

Authors' contributions
MAA-O and MHB conceived of the presented idea. UK with help and support from MAA-O conducted the experiments and performed the numerical simulations. MAA-O, MHB, and MKR developed the mechanistic model. UK and MAA-O developed the manuscript with support from MHB and MKR. All authors read and approved the final manuscript.

Author details
[1] Civil and Environmental Engineering Department, King Fahd University of Petroleum and Minerals (KFUPM), Dhahran 31261, Saudi Arabia. [2] Center for Engineering Research, Research Institute, King Fahd University of Petroleum, & Minerals (KFUPM), Dhahran 31261, Saudi Arabia.

Publisher's Note
Springer Nature remains neutral with regard to jurisdictional claims in published maps and institutional affiliations.

Al-Osta *et al. Int J Concr Struct Mater* (2018) 12:46

Page 20 of 20

References

ACI Committee, 318-14. (2014). Building code requirements for structural concrete and commentary.

ACI-ASCE Committee 352. (2002). *Recommendations for design of beam-column connections in monolithic reinforced concrete structures*. Farmington Hills: American Concrete Institute.

Al-Osta, M., Al-Khatib, A., Baluch, M., Azad, A., & Rahman, M. (2017). Performance of hybrid beam-column joint cast with high strength concrete. *Earthquakes and Structures, 12*(6), 603–617.

Antonopoulos, C. P., & Triantafillou, T. C. (2003). Experimental investigation of FRP strengthened RC beam-column joints. *ACSE Journal of Composites for Construction, 7*(1), 39–49.

Bakir, P. G., & Boduroglu, H. M. (2002). A new design equation for predicting the joint shear strength of monotonically loaded exterior beam-column joints. *Engineering Structures, 24*(8), 1105–1117.

Barnes, M. & Jigoral, S. (2008). Exterior non-ductile beam column joints. University of California, Berkeley, PEER/NEESREU Research Report.

Birtel V., & Mark P. (2006). Parameterized finite element modeling of RC beam shear failure. ABAQUS Users' Conference.

Clyde, C., Pantelides, C. P., & Reaveley, L. D. (2000). Performance-based evaluation of exterior reinforced concrete building joints for seismic excitation. PEER Report 2000/05 University of California, Berkeley.

Ghobarah, A., & Said, A. (2001). Seismic rehabilitation of beam-column joints using FRP laminates. *Journal of Earthquake Engineering, 5*(1), 113–129.

Hakuto, S., Park, R., & Tanaka, H. (2000). Seismic load tests on interior and exterior beam-column joints with substandard reinforcing details. *ACI, Structural Journal, 97*(1), 11–25.

International Federation for Structural Concrete (fib). (2010). Fib model code for concrete structures, 1.

Li, B., Lam, E. S. S., Wu, B., & Wang, Y. (2015). Effect of high axial load on seismic behavior of reinforced concrete beam-column joints with and without strengthening. *ACI, Structural Journal, 112*(6), 713–723.

Masi, A., Santarsiero, G., Mossucca, A., & Nigro, D. (2014). Influence of axial load on the seismic behavior of RC beam-column joints with wide. *Applied Mechanics and Materials, 508,* 208–214.

Masi, A., Santarsiero, G., & Nigro, D. (2013). Cyclic tests on external RC beam-column joints: role of seismic design level and axial load value on the ultimate capacity. *Journal of Earthquake Engineering, 17*(1), 110–136.

Pantelides, C. P., Clyde, C., & Reaveley, D. L. (2002). performance-based evaluation of exterior reinforced concrete building joints for seismic excitation. *Earthquake Spectra, 18*(3), 449–480.

Pantelides, C., Okahashi, Y., & Reaveley, L. (2008). Seismic rehabilitation of reinforced concrete frame interior beam-column joints with FRP composites. *ASCE, Journal of Composites for Construction, 12*(4), 435–445.

Sarsam, K. F., & Phillips, M. E. (1985). The shear design of in situ reinforced beam-column joints subjected to monotonic loading. *Magazine of Concrete Research, 37*(130), 16–28.

Tran, M. T. (2016). Influence factors for the shear strength of exterior and interior reinforced concrete beam-column joints. *Sustainable Development of Civil, Urban and Transportation Engineering Conference, Procedia Engineering, 142,* 63–70.

Vollum, R. L., & Newman, J. B. (1999). The design of external, reinforced concrete beam column joints. *The Structural Engineer, 77*(23–24), 21–27.

Wong, H.F. (2005). Shear strength and seismic performance of non-seismically designed reinforced concrete beam-column joints. PhD Dissertation, Department of Civil Engineering, the Hong Kong University of Science and Technology.